Electrical Power and Energy Systems 153 (2023) 109352

Contents lists available at ScienceDirect

International Journal of Electrical Power and Energy Systems

journal homepage: www.elsevier.com/locate/ijepes

Probabilistic machine learning aided transformer lifetime prediction framework for wind energy systems

Jose I. Aizpurua [a,b,*], Rafael Peña-Alzola [c], Jon Olano [a], Ibai Ramirez [a], Iker Lasa [d], Luis del Rio [d], Tomislav Dragicevic [e]

[a] Mondragon University, Electronics & Computer Science Department, Arrasate, Spain
[b] Ikerbasque, Basque Foundation for Science, Bilbao, Spain
[c] University of Strathclyde, Electronic & Electrical Engineering Department, Glasgow, UK
[d] Ormazabal Corporate Technology, Amorebieta-Etxano, Spain
[e] Technical University of Denmark, Department of Wind and Energy Systems, Lyngby, Denmark

ARTICLE INFO

Keywords:
Transformer
Wind energy
Reliability
Machine learning
Surrogate modelling
Power curve

ABSTRACT

Accurate lifetime prediction of transformers operated in power grids with renewable energy systems is a challenging task because it requires a large amount of data that is not usually available. In the case of wind energy, this complexity is intensified with the stochastic ageing process influenced by the intermittency of the wind and weather conditions. Existing models make use of detailed power topologies to evaluate transformer stress profiles and associated degradation. However, this modelling approach requires high computational resources and long simulation times. In this context, this paper presents a lifetime prediction model for transformers designed through probabilistic machine learning, thermal modelling and ageing analysis. The proposed model is compared with synthetic wind-to-power detailed simulations of a wind farm and validated with real data. The lifetime prediction is evaluated with different mission profile estimates and results show that the accuracy of the probabilistic machine learning model is very high, with an error of 0.47% for the median value and 80% prediction interval errors within 6%–7% with respect to observations. Moreover, there is a substantial reduction in the simulation time and memory requirements when compared to the synthetic model. A detailed sensitivity analysis demonstrates the influence on transformer ageing of different overloading strategies, thermal constants and the geographic location of the wind farm.

1. Introduction

Renewable energy sources (RESs) play a key role in the transition towards a decarbonized economy, and their reliable and efficient integration into the power grid is crucial for the safe operation of power and energy systems. Wind energy (WE) is the most mature RES, with a total of 837 GW of wind power installed worldwide [1]. The expected lifetime of a WE plant is around 15–20 years, and the health status of WE components along with operation and maintenance costs (O&M) drive lifetime extension decisions [2]. Prognostics and health management (PHM) solutions reduce O&M costs and support lifetime extension of assets through e.g. early detection of anomalies [3], health state diagnostics [4], prediction of remaining useful life (RUL) [5] and condition-based maintenance solutions [6].

Different PHM and reliability models have been proposed mainly to evaluate the lifetime of mechanical components of WE systems [7]. However, PHM for the electrical system could play an important role in the O&M cost reduction. In particular, transformers are key components that enable the integration of WE into the grid [8]. There are different factors that influence transformer degradation [9]. Well-established transformer O&M practices include dissolved gas analysis and offline testing as in [10]. Insulation degradation is the most penalizing phenomenon that can cause power outages [11]. Transformer insulation lifetime depends on the hottest-spot temperature (HST), which changes with the transformer loading and ambient temperature. In turn, the transformer loading and ambient temperature are specific to the operation location and usage profiles.

1.1. Related work

An effective O&M planning strategy for WE systems requires an accurate prediction of the generated wind power to estimate the associated operation and ageing profiles. However, this is a challenging task and different predictive models have been developed to improve

* Corresponding author at: Mondragon University, Electronics & Computer Science Department, Arrasate, Spain.
E-mail addresses: jiaizpurua@mondragon.edu (J.I. Aizpurua), rafael.pena-alzola@strath.ac.uk (R. Peña-Alzola), jon.olano@alumni.mondragon.edu (J. Olano), iramirezg@mondragon.edu (I. Ramirez), ilo@ormazabal.com (I. Lasa), lre@ormazabal.com (L. del Rio), tomdr@dtu.dk (T. Dragicevic).

https://doi.org/10.1016/j.ijepes.2023.109352
Received 24 February 2023; Received in revised form 8 June 2023; Accepted 29 June 2023
Available online 12 July 2023

Nomenclature

η	Wind turbine efficiency [–]
$\hat{f}_t^k$	K-th feature, at instant t
$\hat{P}_t$	Estimated power at instant t [W]
ω	Rotor speed [rpm]
$\overline{m}$	Mean performance [–]
ψ_i	Logistic regression parameters [–]
ρ	Air density [kg/m^3]
C_p	Power coefficient [W]
$i(t)$	Load at instant t [A]
$i_r(t)$	Rated load at instant t [A]
i_d	Direct current [A]
i_q	Quadrature-current [A]
i_{rd}	Direct rotor current reference [A]
i_r	Rotor current [A]
i_s	Stator current [A]
N	Total number of wind turbines
p_i	Power generated by the ith turbine [W]
q_ϕ	ϕ quantile [–]
R	Rotor radius [m]
S	Wind speed [m/s]
T_e*	Torque reference [N]
v	Wind speed at hub height [m/s]
v_g	Grid voltage [V]
v_{dc}	DC-link voltage [V]
v_d	Direct voltage [V]
v_q	Quadrature voltage [V]
v_{rd}	Direct rotor voltage reference [V]
v_{rq}	Quadrature rotor voltage reference [V]
$W_1(F_y, F_{\hat{y}})$	Wasserstein distance between distributions [–]
$\Delta\theta_H(t)$	HST rise, over top-oil temperature at instant t [°C]
$\Delta\theta_{H,R}(t)$	HST rise at rated load, at instant t [°C]
τ_{TO}	Oil time constant [min]
τ_W	Winding time constant [min]
$\theta_H(t)$	Hottest spot temperature at instant t [°C]
$\theta_A(t)$	Ambient temperature at instant t [°C]
$\theta_{TO}(t)$	Top-oil temperature at instant t [°C]
K(t)	Normalized load at t [p.u.]
k_{11}, k_{21}, k_{22}	Thermal constants [–]
R	Ratio of load losses to no load losses [W]
V(t)	Insulation ageing rate at t [h]
x	Oil exponent constant [–]
y	Winding exponent constant [–]

the prediction accuracy of the wind resource and the generated power e.g. [12,13].

The dynamic power generation of WE systems causes varying transformer thermal stress profiles that result in intermittent ageing profiles. This can lead to risk-averse or risk-seeking O&M decisions, e.g. the overvoltage requirement is 115% of rated voltage in wind turbine transformers [8]. In this direction, different transformer thermal rating solutions [14,15], interactions involving wind farms [16], and optimal wind farm sizing solutions have been proposed [17].

There exist detailed analytic models for wind-farm power flow assessment that include different dynamics, such as electrical transient as a result of the turbulence [18]. These modelling methods can be used to accurately estimate transformer loading dynamics in the sub-second timescale. However, if these solutions are used for long-term lifetime analysis, the model resolution becomes computationally unfeasible due to the underlying non-linear modelling with a large number of space-state equations and dense function evaluations. The simulation time becomes excessive and the memory requirements impractical.

In this context, surrogate models for accelerated representation of mission profiles, that cover a manageable timescale with sufficient accuracy and without demanding excessive computational and memory requirements, are practical and effective solutions. Surrogate models have been used for different engineering solutions including the accelerated design of wind turbines [19] and hydropower turbines [20], offshore wind turbine fragility analysis [21], or wind turbine blade fatigue prediction [22]. In the area of transformer lifetime assessment, there are improved top-oil temperature estimation methods using surrogate methods [23]. However, to the best of authors' knowledge, surrogate models have not been used for the accelerated transformer mission profile estimation and its propagation to estimate the transformer lifetime. Efficient power flow processing algorithms can enhance and accelerate the load estimation process [24]. However, in order to capture the influence of different covariates on the load estimate, probabilistic machine learning (ML) algorithms are strong candidates for capturing and modelling power generation and conversion dynamics accurately and efficiently [25,26].

1.2. Contribution and impact

Accordingly, the contribution of this work is the development of a probabilistic ML aided transformer lifetime estimation framework for substation transformers operated in WE systems. This is achieved through surrogate modelling, which accelerates the mission profile estimation and transformer ageing analysis. The proposed methodology provides a practical solution for the analysis of operation conditions and associated mission profiles when evaluating transformer reliability.

The proposed approach is compared with detailed synthetic simulation models and validated with real wind farm data. Obtained results show that the mission profile estimation accuracy of the probabilistic ML model is very high with an error of 0.47% for the median value and 80% prediction interval errors within 6%–7% with respect to wind power observations. Moreover, there is a substantial reduction in the simulation time and memory requirements when compared to the synthetic model. Sensitivity and impact assessments of overloading strategies, thermal constants and geographic location of the wind farm are carried out to discuss key transformer ageing indicators and highlight the applicability of the framework.

1.3. Organization

The remainder of this article is organized as follows. Section 2 presents the proposed approach. Section 3 defines the case study. Section 4 shows the obtained numerical results, Section 5 presents a discussion of the results and the approach, and finally, Section 6 concludes the article.

2. Probabilistic machine learning aided wind farm transformer lifetime approach

Fig. 1 shows the classical transformer lifetime assessment approach for wind farm transformers. The approach starts with the wind power modelling stage, which estimates the generated power based on operation conditions and mission profiles. This process is continued with the transformer thermal modelling stage, which estimates the HST, and finally, this is further propagated to calculate the transformer degradation.

Traditionally, the wind power modelling stage is implemented using domain-specific wind energy models, which include detailed power generation dynamics and high-accuracy results [18]. However, it is

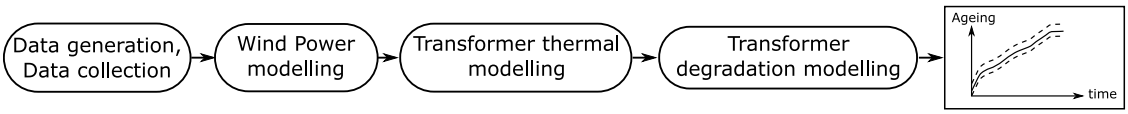

Fig. 1. Classical lifetime estimation framework for wind-farm transformers.

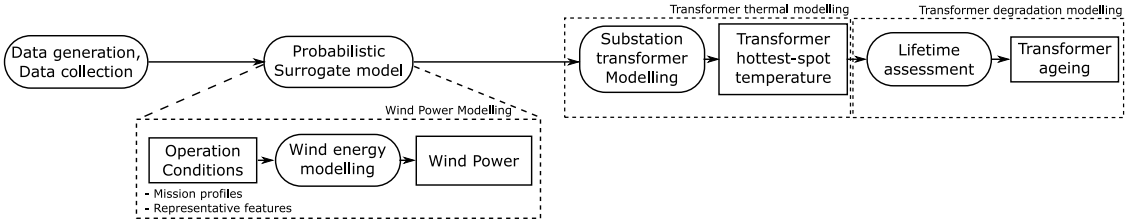

Fig. 2. Probabilistic ML aided lifetime estimation framework for wind-farm transformers.

Table 1
Comparison of domain-specific and surrogate modelling strategies.

Strategy	Accuracy	Memory	Simulation time	Sampling rate
Domain-specific modelling	High	High	High	High
Surrogate model	High	Low	Low	Lower

possible to capture the wind power generation dynamics with an equivalent surrogate model so that it obtains accurate results with a faster computation time and less memory resources. Table 1 compares wind power modelling strategies with respect to accuracy, memory resources, simulation time and sampling rate.

If an accurate surrogate model is obtained, it can be expected that the same equivalent results could be obtained with lower computational and memory costs [19–22]. Note also that the domain-specific model may be able to infer data at a higher sampling rate because it models detailed power generation dynamics. In this direction, this research focuses on the use of probabilistic ML models to capture the uncertainty associated with the power generation process, and propagate it during the subsequent modelling stages [27].

Accordingly, Fig. 2 shows the proposed probabilistic ML aided transformer lifetime estimation framework. The objective of the framework is to generate fast and accurate transformer ageing estimates.

Based on the operation conditions and wind-farm specific power generation and conversion stages, the generated wind power and associated transformer loading can be estimated, *i.e.* mission profiles. This load profile is then used to estimate the transformer thermal stress, which depends on the electrical load and ambient temperature. The thermal stress is then connected with the lifetime model to estimate the impact on transformer ageing, and accordingly, to adopt O&M decisions.

The framework in Fig. 2 becomes the surrogate model that captures the operation and power generation dynamics of the wind farm from available natural resource data. This enables to estimate the degradation trajectories of the substation transformer, including power operation dynamics, in an accelerated manner. This is achieved through an equivalent analytical model that is used to learn operation dynamics in order to emulate them.

2.1. Wind power modelling

The wind is a natural resource with seasonal and year-to-year variations. The power generated by a wind turbine i, p_i, can be estimated as follows [18]:

$$p_i = \frac{1}{2} C_p \rho \pi R^2 v^3 \eta \tag{1}$$

where ρ is the air density [kg/m^3], C_p is the power coefficient [W], R is the rotor radius [m], and v is the wind speed at hub height [m/s]. The factor η models all the overall efficiency of the wind turbine, including the electrical generator and the power electronic converters.

For the case of a wind farm comprising N turbines, the output power is defined as follows:

$$P = \sum_{i \in N} p_i \tag{2}$$

Wind power forecasting is a non-trivial task where a number of factors, such as the geographic location, operation efficiency, sensing equipment and component degradation influence the generated energy [28]. Two different strategies for wind power prediction are designed and evaluated: domain-specific modelling and surrogate machine-learning modelling.

2.1.1. Domain-specific modelling

A synthetic model has been designed to estimate the generated power in the wind farm under different series of wind speeds. Fig. 3 shows the high-level scheme of the analysed wind farm, which comprises the different wind turbines along with the substation transformer that connects the wind farm and the grid. The wind turbines use doubly fed induction generators (DFIG), which is a mature technology of widespread use [29], and constitutes a proper benchmark for decisions on O&M and lifetime extension.

In these turbines, a gearbox connects the hub and the DFIG to accommodate the slow hub rotation with the grid frequency [29]. The stator of the DFIG is directly connected to the grid, whereas the rotor is connected to a back-to-back converter through slip-rings. This arrangement allows obtaining speed variations around the synchronous speed for maximum power point tracking (MPPT) of the wind potential. The main advantage of this configuration is that the power electronic converter is sized to a fraction of the rated power, which results in high efficiency. The main disadvantage is the utilization of slip-rings, which are subject to wear-out and require periodic maintenance [29].

The simulation model for the wind turbine includes the DFIG and the power electronic converters. This model is used to calculate the generated wind power and the load profile of the substation transformer. The wind turbine is modelled using a lookup table that relates the output mechanical power with the wind and the hub speeds. Phasor simulation is used for the DFIG machine, where electrical transients are neglected and only the slow mechanical transients are considered. The DFIG and the power electronic converters are modelled as controlled current sources, with their amplitudes resulting from the phasor simulation.

Fig. 4 shows the control block diagrams corresponding to the detailed synthetic model of the DFIG-based wind turbines. The DFIG is controlled using standard vector control with nested loops. Both

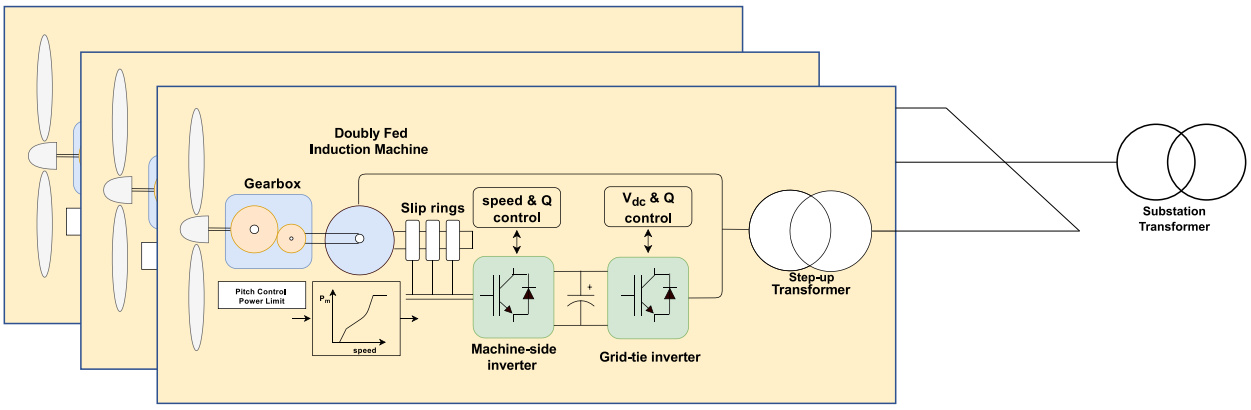

Fig. 3. Scheme of the wind farm with individual DFIGs used in the case study.

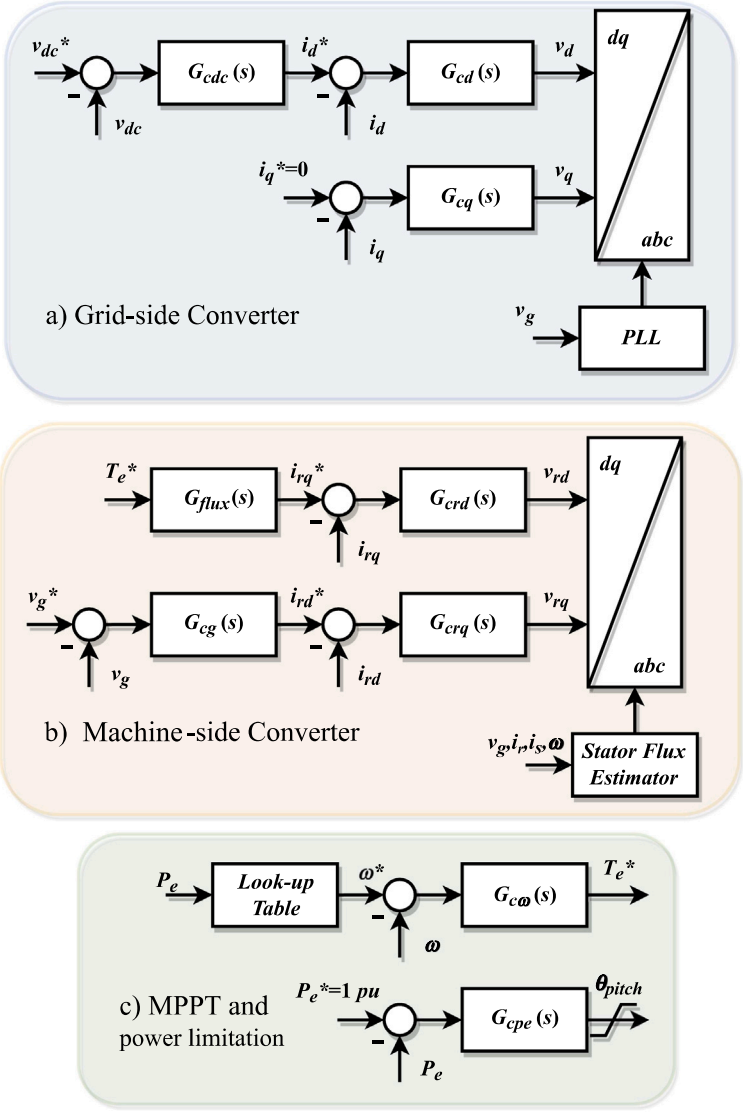

Fig. 4. Control block diagrams corresponding to the detailed synthetic model of DFIG-based wind turbines of the wind farm shown in Fig. 3.

grid-side and converter-side converters use inner loops for dq-current control in order to protect the converter and obtain simplified dynamics.

Fig. 4a shows the control block diagram of the grid-tied inverter. The dq-reference frame is aligned with the direct component of the grid voltage v_g, which is captured by using a digital phase-locked loop (PLL). The controller regulates the DC-link voltage v_{dc} in the back-to-back converter by modifying the d-current reference i_d^*. The reactive power reference for the grid-tie inverter, directly regulated with the q-current reference i_q^*, is set to zero for unity power factor. The outputs of the

regulators for the direct and quadrature currents i_d and i_q determine the direct and quadrature voltage references v_d and v_q to the PWM modulator of the grid-tie inverter, respectively.

Fig. 4b shows the control block diagram for the machine-side inverter. The rotating framework for the dq-components is the DFIG stator flux, which allows regulating the machine reactive power along with the electrical torque [30]. The stator flux is estimated from the measured stator and rotor currents i_s and i_r, grid voltage v_g and rotor speed ω. The reactive power reference is determined by the direct rotor current reference i^*_{rd} and is the output of a controller that regulates the voltage droop amplitude at the grid terminals v_g. The torque reference T^*_e is directly proportional to the quadrature current reference i^*_{rq} and the stator flux. The torque reference T^*_e is provided by the MPPT of the wind turbine. The outputs of the regulators for the direct and quadrature rotor currents i_{rd} and i_{rd} determine the direct and quadrature voltage references v_{rd} and v_{rq} to the PWM modulator of the machine-side inverter, respectively.

Fig. 4c shows the control block diagram of the MPPT and the power limitation. It is based on a lookup table relating the DFIG output power P_e with the hub speed of the wind turbine ω. The output speed ω^* of this lookup table is the reference input of the speed controller, whose output is the torque reference T^*_e. For low wind speed, the blade pitch angle θ_{pitch} remains constant and is set to zero. When the turbine reaches its maximum production, a regulator changes the blade pitch angle in order to limit the power output for higher wind speeds.

The wind farm model is modelled as the aggregation of individual DFIG wind turbines (cf. Fig. 3), each one with the control shown in Fig. 4.

2.1.2. Surrogate ML modelling

Many different methodologies have been proposed in the area of probabilistic wind power forecasting [27]. In contrast, probabilistic forecasting methodologies are just emerging in the area of transformer lifetime modelling [31]. Inspired by the capability of modelling and propagating uncertainty information associated with the modelled process, this research is focused on probabilistic wind power estimates. They will be used to quantify the probabilistic transformer stress and evaluate the transformer ageing under different operation profiles.

Namely, the estimated power at instant t, $\hat{P}_t$, is estimated from indirect covariates:

$$\hat{P}_t = g(f_t^1, \ldots, f_t^K); \tag{3}$$

where f_t^i contains ith feature, $f_t^i \in F$. The set $F = \{f_t^1, \ldots, f_t^K\}$ denotes the set of features for the best estimation of the measured wind power at t, P_t, by using the predictive model $g(.)$, which aims at minimizing the difference between observations and predictions.

The operational variables that affect wind energy are stochastic, and therefore, load estimation models should integrate uncertainty information inherent in the energy generation and conversion process. Accordingly, a probabilistic load forecasting model has been designed. Without loss of generality and to show the capability of connecting and propagating probabilistic wind power estimates with transformer lifetime models, probabilistic estimates will be based on Quantile Regression Forest (QRF) models [32]. QRF models are based on Random Forests (RF) with a powerful predictive performance [33]. A RF grows an ensemble of regression trees using M independent observations, $\{y, x_i\}_{i=1}^M$, where y is the wind power, P_t, $x_i \in X$ are the prediction variables, and M is the length of training data. QRFs draw prediction intervals from RF predictions. The prediction becomes a conditional distribution function $F(y|X = x_i)$, *i.e.* probability of the predicted wind power value y, given the prediction variables X, which is approximated by the weighted mean of x_i over the observations:

$$\hat{F}(y|X = x_i) = \sum_{i=1}^{M} w_i(x_i) 1_{\{y<y_i\}} \tag{4}$$

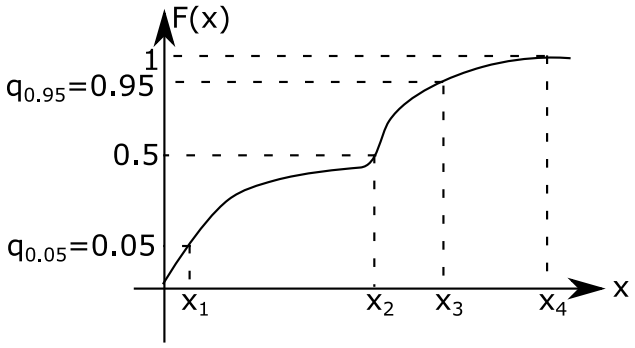

Fig. 5. Cumulative distribution function (CDF) and quantiles.

where $w_i(x_i) = K^{-1} \sum_{k=1}^{K} w_i(x_i \theta_k)$ is the weighted vector and $1_{\{.\}}$ is an indicator function.

The ϕ-quantile, $q_\phi(x_i) = \phi$, is defined such that the probability of $y < q_\phi(x_i) = \phi$. That is, a quantile of order ϕ is a value where the distribution function crosses ϕ. Quantiles provide a complete distribution information of y as a function of explanatory features X. For example, for a feature set, X, and target variable y, 90% prediction intervals (PI) are estimated as:

$$PI(X) = [q_{0.05}(y|x = X), q_{0.95}(y|x = X)] \tag{5}$$

Fig. 5 shows a distribution function example, including quantiles, where the area under the interval $[x_1, x_3]$ covers 90% PI.

Using quantiles and interpolation methods, it is possible to build a CDF. In this case, the monotonic piecewise interpolation method was used [34].

The main criteria to evaluate the probabilistic forecasts is the continuously ranked probability score (CRPS). From the probabilistic forecast PDF, $f(z)$, with its cumulative distribution function (CDF), $F(z)$, and observation y, the $CRPS(F, y)$ is defined as [35]:

$$CRPS(F, y) = \int_{\mathbb{R}} (F(z) - \mathbb{1}\{y \le z\})^2 \, dz \tag{6}$$

where $\mathbb{1}\{y \le z\}$ is the indicator function, which is one if $y \le z$ and zero otherwise.

The CRPS calculates the discrepancy between the forecast CDF and the empirical CDF of the observation $\mathbb{1}\{y \le z\}$, which is considered as a step function because the observations y are deterministic values. The CRPS is a metric better suited for categorizing the predictive power of probabilistic models that generate a PDF as a prediction because it quantifies the error of each probabilistic value with respect to the observation [35]. Other metrics, such as the mean average error (MAE), are based on error values from deterministic point estimates. Thus, these metrics need to quantify the MAE value for every quantile in order to have an overall idea of the predictive power.

The algorithm QRF is implemented in the package `quantregForest` of the R software environment for statistical computing. The model tuning has been carried out from a predefined grid of parameters including the number of variables to try for each split when growing a tree (mtry), minimal number of instances in each terminal node, determining the minimal number of instances per node (nodesize) and number of trees to be grown (ntree). These parameters aim at preventing overfitting and were considered as follows: nodesize = [5, 10, 20], mtry = [1, 2, 3] and ntree = [10, 100, 1000, 2000].

2.2. Transformer thermal modelling

According to the IEC 60076-7, the transformer HST can be defined as follows [36]:

$$\Theta_{\mathrm{H}}(t) = \Theta_{\mathrm{TO}}(t) + \Delta\Theta_{\mathrm{H}}(t) \tag{7}$$

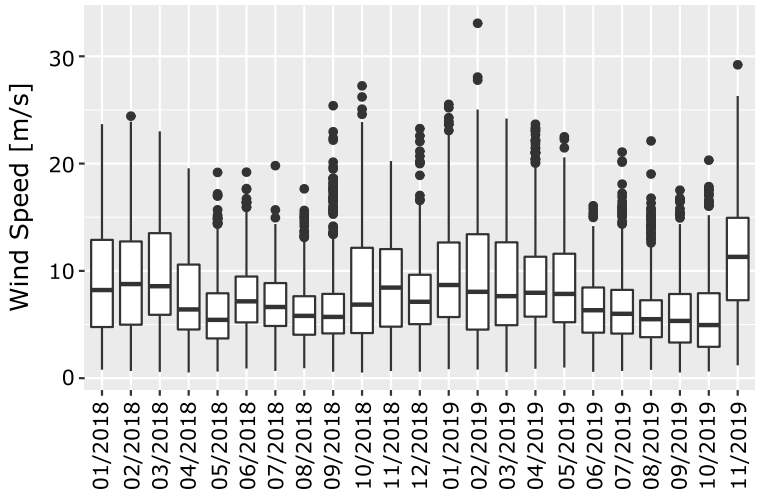

Fig. 6. Box plots of wind speed for the monthly averages of measurement data in the Jelinak wind farm.

where $\Theta_{\mathrm{H}}(t)$ is the HST at instant t [°C], $\Delta\Theta_{\mathrm{H}}(t)$ is the HST rise over top-oil temperature [°C] and $\Theta_{\mathrm{TO}}(t)$ is the top-oil temperature [°C]. For small Δt, differential equations can be approximated to difference equations and the top-oil temperature (TOT) is calculated as follows:

$$\Theta_{\mathrm{TO}}(t) = D\Theta_{TO}(t) + \Theta_{\mathrm{TO}}(t-1) \tag{8}$$

$$D\Theta_{\mathrm{TO}}(t) = \frac{\Delta t}{k_{11}\tau_{TO}}\left[\Delta\Theta_{H,R}\left(\frac{1+K(t)^2R}{1+R}\right)^{x} + \Theta_A(t) - \Theta_{\mathrm{TO}}(t-1)\right] \tag{9}$$

where $K(t) = i(t)/i_{\mathrm{r}}$, $i(t)$ being the load at instant t [per unit] and i_{r} the rated load [A], R is the ratio of load losses to no-load losses [W], x is the oil exponent constant that models the exponential power of total losses with respect to TOT heating, τ_{TO} is the oil time constant [minutes], $\Delta\Theta_{\mathrm{H,R}}$ is the HST rise at rated load [°C], k_{11} is a thermal constant determined through experimentation, and finally $\Theta_{\mathrm{A}}(t)$ is the ambient temperature [°C].

Similarly, the HST can be calculated as follows:

$$\Delta\Theta_{H_i}(t) = D\Delta\Theta_{H_i}(t) + \Delta\Theta_{H_i}(t-1) \tag{10}$$

for i = {1,2}, where

$$D\Delta\Theta_{H_1}(t) = \frac{\Delta t}{k_{22}\tau_w}\left[k_{21}\Delta\Theta_{\mathrm{H,R}}K(t)^y - \Delta\Theta_{H_1}(t-1)\right] \tag{11}$$

$$D\Delta\Theta_{H_2}(t) = \frac{k_{22}\Delta t}{\tau_{\mathrm{TO}}}\left[(k_{21}-1)\Delta\Theta_{\mathrm{H,R}}K(t)^y - \Delta\Theta_{H_2}(t-1)\right] \tag{12}$$

where τ_{w} is the winding time constant [minutes], $\Delta\Theta_{\mathrm{H,R}}$ is the HST rise at rated load [°C], y is the winding exponent constant that models the loading exponential power with the heating of the windings, finally k_{21} and k_{22} are the transformer thermal constants.

2.3. Transformer degradation modelling

The IEC 60 076-7 standard defines insulation paper ageing rate at time t, $V(t)$, as follows [36]:

$$V(t) = 2^{(98-\Theta_H(t))/6} \tag{13}$$

which is based on the hypothesis that a unit of life is consumed at a rate of 98 °C.

3. Case study

The case study focuses on the Jelinak wind farm, located in the region of Split-Dalmatia (Croatia). The wind farm comprises 20 wind turbines (AW-1500, DFIG) with a rated capacity of 30 MW. Fig. 3 shows the wind-farm basic components, including step-up transformers and wind-farm integration transformers. This work focuses on the reliability analysis of integration transformers that connect the wind farm to the grid.

The monitored data covers the period 01/2018–11/2019 and includes hourly sampled wind speed, direction, density and the generated power [37]. Figs. 6, 7, and 8 show the box plots of power, wind speed and temperature for the monthly averages of measurement data.

It can be observed that during 2018, there was a decrease in the wind speed through April and May in addition to that typical of the summer months of July, August and September. In 2019, the decreasing wind speed trend started in June and lasted till October. This is directly translated into the generated power of the wind farm (cf. Fig. 7). As for the ambient temperature, the highest temperatures were recorded during June, July and August months in 2018 and 2019.

Fig. 9 shows the rated power curve of the Jelinak wind farm. The integration transformer operated in the wind farm is assumed to be rated at the 90% of the wind farm rating, with the following design parameters [36]: $k_{11} = 0.75$, $k_{21} = 2.32$, $k_{22} = 2.05$, $\Delta\Theta_{H,R} = 15.1$ [°C], $\Delta\Theta_{TO,R} = 54.26$ [°C], Load losses/No load losses = 9800/842 [W], $\tau_0 = 180$ [min], and $\tau_w = 4$ [min].

4. Numerical experiments

This section will carry out numerical experiments for the wind power modelling, the transformer lifetime analysis as well as a sensibility analysis to assess the influence of the different parameters in the estimates.

4.1. Wind power modelling

This subsection focuses on the wind power modelling. Simulation results for the synthetic wind farm model will be shown. This outcome will enable the design of the proposed QFR model. The model validation is verified by comparing the power curves.

4.1.1. Synthetic wind farm model

The synthetic simulation model presented in Section 2.1.1, implemented in Matlab/Simulink [38], was used to generate the output electrical power of the wind farm from the wind speed data.

The phasor mode was selected for the synthetic simulation because the sampling rate of the wind speed data is one hour. This approach neglects fast transients from the power electronic converters and the electrical machine, and only considers the mechanical dynamic equations. Thus, the differential equations of the electrical components become algebraic and the simulation speed increases by using a step

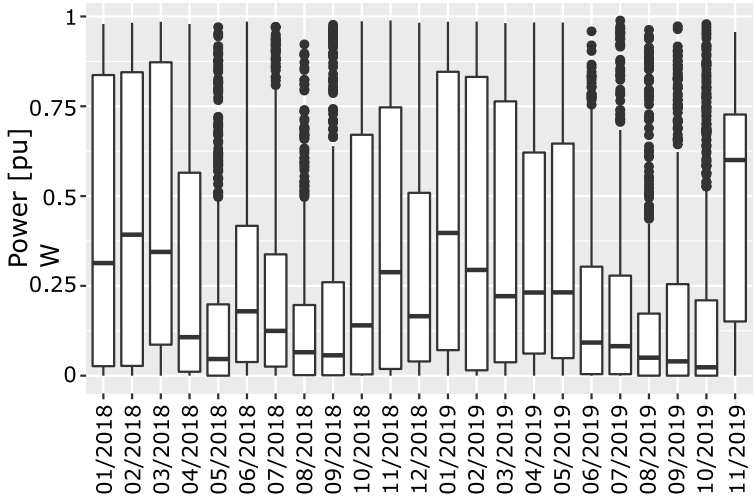

Fig. 7. Box plots of power for the monthly averages of measurement data in the Jelinak wind farm.

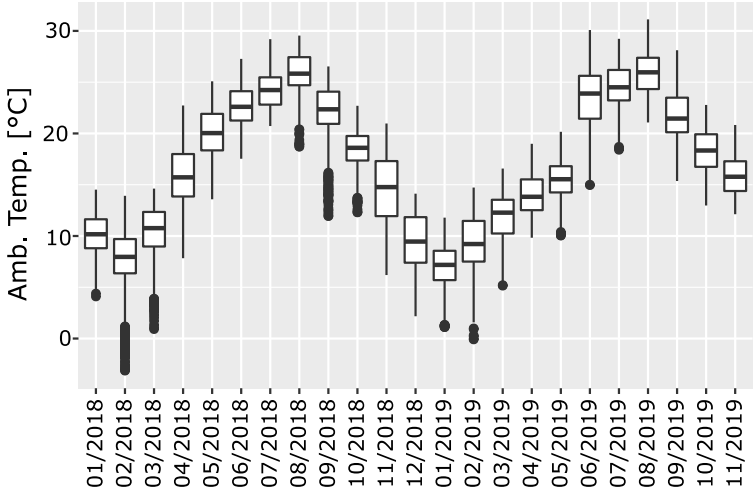

Fig. 8. Box plots of ambient temperature for the monthly averages of measurement data in the Jelinak wind farm.

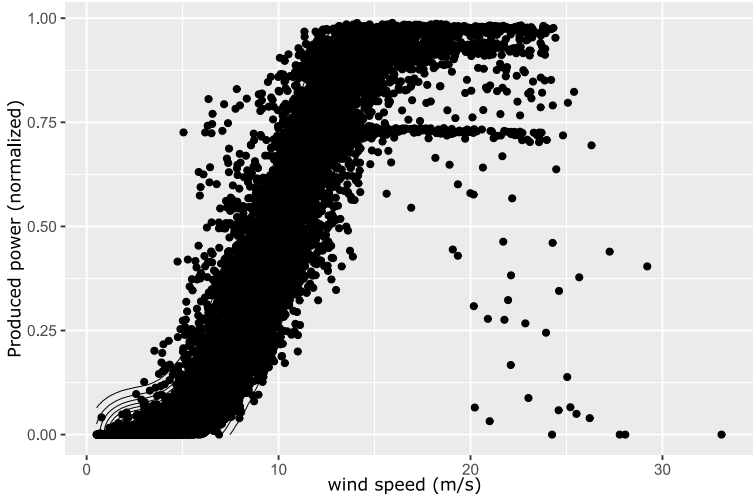

Fig. 9. Normalized power curve of Jelinak (01/01/2018–28/11/2019).

Table 2
CRPS values for 10-fold CV results for different models (mean values).

Model[a]	$fold_1$	$fold_2$	$fold_3$	$fold_4$	$fold_5$	$fold_6$	$fold_7$	$fold_8$	$fold_9$	$\overline{mean}$	Holdout
(#1)	4.6	3.1	3.2	2.6	3.4	2.3	2.2	2.9	3.06	3.08	3.92
(#2)	3.57	2.47	2.64	2.51	3.18	2.22	2.28	2.82	3.17	**2.76**	3.44
(#3)	4.26	3.1	2.96	2.79	3.71	2.72	2.61	3.3	3.5	3.2	3.88

[a]Model covariates: (#1): {wind speed, wind direction, wind density}; (#2): {wind speed, wind direction}; (#3): {wind speed, wind density}.

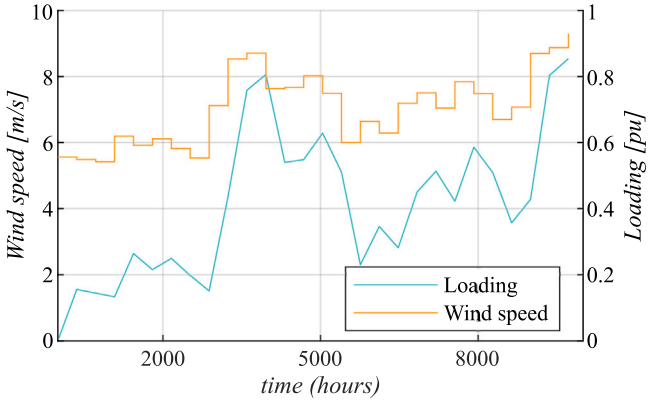

Fig. 10. Hourly sampled transformer power loading profiles (01/12/2018–28/11/2019).

size equal to the fundamental period (in seconds, one over the fundamental frequency of 50–60 Hz). The output values show variations of phasor magnitudes and angles due to the machine speed variations.

To cope with the high computational and storage costs, the whole year of wind speed data was simulated partitioning data month-by-month with an hourly resolution and the corresponding results were stored in files. Fig. 10 shows the generated transformer loading profiles along with the input wind speed profile for a full year.

4.1.2. Machine-learning based modelling

The design and validation of the QRF model is based on training, validation and holdout testing set. One year long data, including different covariates, have been used to model, evaluate and select the QRF model with the best covariates. Sequential 10-fold cross validation (CV) procedure was used [39], where different lengths of the data, divided into equidistant blocks b_i, have been used for training and testing the model, *i.e.* f_1: train $\{b_1\}$, test $\{b_2\}$, f_2: train $\{b_1, b_2\}$, test $\{b_3\}$, until f_9: train $\{b_1, \ldots, b_9\}$, test $\{b_{10}\}$. The CV procedure implements iterative training and validation on the parameters defined in the grid-search strategy (cf. Section 2.1.2) and reports the best model based on the loss function. This CV strategy enables the generalization of the predictive performance results by examining the models under different training and testing scenarios. The number of folds incurs a bias–variance tradeoff compromise and 10-fold CV have been shown to yield error estimates that suffer neither from high bias nor high variance [40].

The model with the best mean performance ($\overline{mean}$) has been selected for tuning and testing. Finally, the holdout testing set (holdout), comprised of one year data, which matches with the synthetic wind-farm model period (cf. Fig. 10), has been used to obtain the unbiased estimation of the generalization error. Fig. 11 shows the training, testing and validation strategy.

Using the formulation in Eq. (3) a set of different covariates have been assessed to evaluate the predictive power of different variables and proceed with the most accurate model. Namely, model (#1) includes wind speed, wind direction and wind density measured at instant t, model (#2) includes wind speed and wind direction measured at instant t, and finally, model (#3) includes wind speed and wind

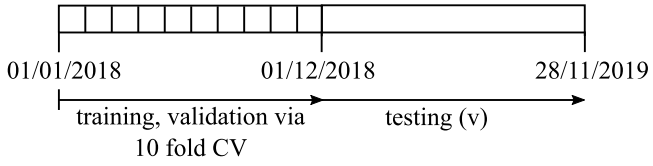

Fig. 11. Training, testing and validation strategy.

density measured at instant t. It may have been possible to infer additional features through e.g. decomposition methods [41,42], and select using e.g. mutual information criteria [43]. However, direct measurements inferred from Eq. (1) have been used to avoid further computational complexity in the overall methodology. Table 2 shows the obtained results quantified through the continuously ranked probability score (CRPS), which generalizes mean average error for probabilistic predictions.

It can be observed that the model with the best performance uses wind speed and direction as input variables in agreement with the underlying physical process. This configuration has been used for subsequent analysis stages. Fig. 12 shows the probabilistic load results for the last week of operation and the corresponding temperature estimates.

4.1.3. Model validation and comparison

The validation strategy focuses on the power curve modelling and comparison. Power curves are compared through parameterized functions using the logistic model [44]:

$$P(S) = \frac{\psi_1}{1 + exp((\psi_2 - S)/\psi_3)} \tag{14}$$

where P is power, S is wind speed, and ψ_1, ψ_2 and ψ_3 are parameters fitted through optimization.

Individual power curve models have been adjusted for measurements, synthetic data, and ML model data (including different PI levels) through (14) and using one-year data (cf. Fig. 10). Fig. 13 shows the logistic function results for the analysed models.

It can be observed that the performance of the adjusted models with respect to observations are very similar, with differences arising from the deterministic nature of the simulation model and realistic operation of the Jelinak wind farm, which may have gone through failures, updates, and different phenomena not captured in the simulation model.

The distance quantification between the fitted functions, which can be effectively seen as the distance between two cumulative distribution functions (CDF), enables the error quantification. In this direction, this work focuses on the implementation of the Wasserstein distance [45], W_1, which measures the distance between two CDFs and has been widely implemented for machine learning applications, e.g. [46,47]:

$$W_1(F_y, F_{\hat{y}}) = \int_{\mathbb{R}} |F_y(x) - F_{\hat{y}}(x)| dx \tag{15}$$

where $F_y(x)$ is the parametric power curve function of the observed data and $F_{\hat{y}}(x)$ is the function of the simulation model (synthetic or ML). Table 3 displays a comparison of error, computation and memory resources.

Therefore, the designed QRF is used for subsequent reliability analyses to evaluate the influence of different operation profiles on the transformer lifetime.

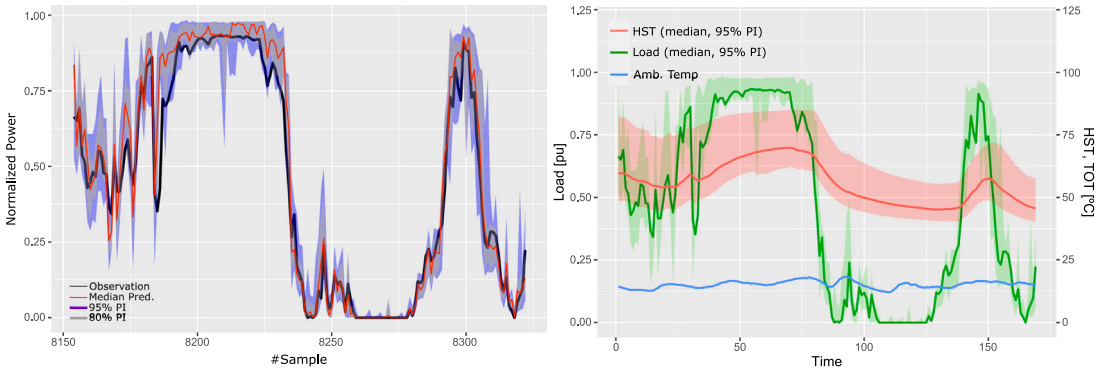

Fig. 12. Left: Probabilistic load predictions. Right: TOT and HST estimates.

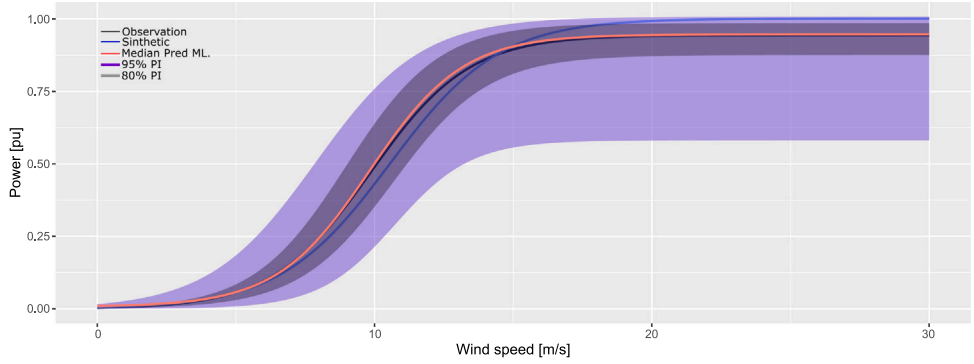

Fig. 13. Comparison of power curves (12/2018–11/2019).

Table 3
Comparison of accuracy and computation resources for the synthetic and ML-reliability models.

Model	W_1	Simulation time [min]	Memory [GB]
Synthetic	0.035	72.06	9.88
ML median	0.0047		
ML 95% PI	[0.11, 0.26]	0.9	2.53
ML 80% PI	[0.06, 0.07]		

Table 4
Transformer cumulative ageing (median, 98% PIs) for different loading strategies (in hours).

Loading	Ageing at 31/12/2018	Ageing at 28/11/2019
90%	26.52, [6.46–70.42]	49.33, [12.52–138.37]
100%	43.69, [7.09–140.83]	80.02, [13.77–279.57]
110%	78.37, [7.89–309.75]	141.89, [15.34–622.1]
120%	391.3, [9.5–1198.22]	449.1, [18.54–2451.71]

4.2. Transformer thermal and degradation analysis

The operation profiles are determined by the QRF and the transformer lifetime model, which includes wind speed, wind direction and ambient temperature variables. Available data has been used to estimate the corresponding HST and associated ageing. Fig. 14 shows the HST and associated ageing degradation predictions.

It can be observed from Fig. 14 that, at the end of the testing period, the median cumulative ageing is of 49.33 h and 95% PIs are within [23.32, 115.18] h. Under these design and operation conditions, the ageing of the transformer insulation is mild. It can be also observed that the uncertainty around the ageing prediction increases as the prediction horizon increases.

4.3. Sensibility analysis

In order to examine the influence of different parameters on the transformer reliability, a sensitivity analysis is presented for assessing the impact of overloading strategies, transformer lifetime estimation parameters and the geographic location.

4.3.1. Overloading strategies

Considering that the transformer ageing is mild under the analysed rating conditions, the impact of the rated power has been further tested. These cases are aligned with the system operator decisions, who can modify the transformer overloading strategies depending on the lifetime assessment. Fig. 15 shows the transformer accumulated ageing for different loading strategies resulting from modifying the transformer rating through transformer thermal modelling and transformer degradation blocks shown in Fig. 2.

It can be observed in Fig. 15 that, when changing the rated power from 90% to 120%, the degradation of the transformer is affected. Table 4 synthesizes the transformer cumulative ageing results at different instants and for different loading strategies.

As expected, it can be inferred from Table 4 that the loading increase is directly related to the transformer ageing. However, it should be noted that the ageing is not proportional to the power increase as the 110% increase leads to almost tripling the ageing.

4.3.2. Thermal constants

Observing the results obtained for different loading strategies, a sensibility analysis of the thermal characteristics has been performed to examine the influence of design parameters on the transformer degradation. In order to perform the sensibility analysis, the influence of the oil time constant (τ_o) and winding time constant (τ_w) on the transformer degradation have been analysed under base loading and overloading conditions. These variables are dependent on the physical

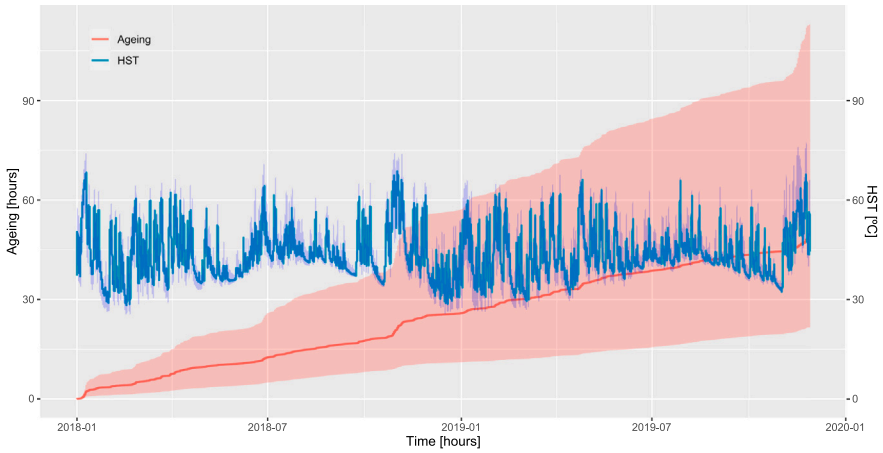

Fig. 14. Cumulative ageing and HST estimate (period 01/01/2018–28/11/2019).

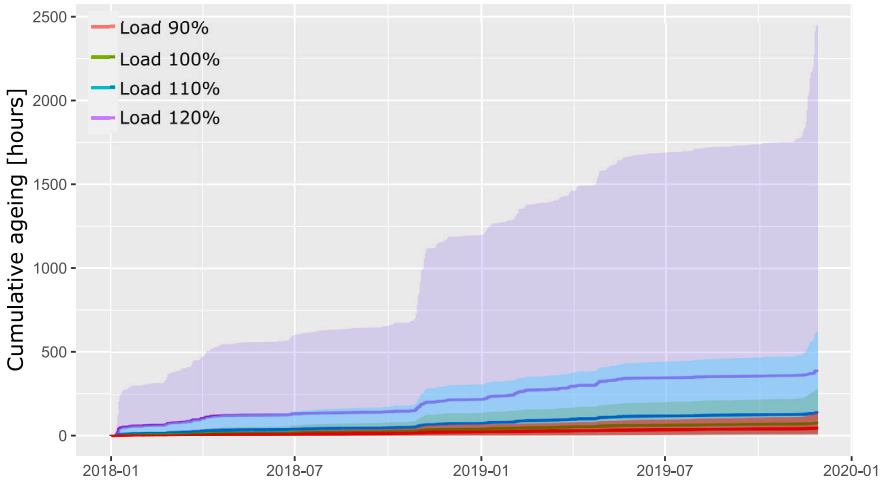

Fig. 15. Transformer ageing under different rated power hypotheses (median, 98% PIs).

structure of the transformer insulation and the materials used to build it, and vary according to the transformer design.

Taking into account different transformer loading strategies, different combinations of thermal constant values (τ_w and τ_o) have been evaluated. Fig. 16 shows the influence on ageing for 90% loading case. The highlighted point indicates the results of the previous test conditions with fixed values of τ_w and τ_o (cf. Table 4)

It can be observed that effectively the thermal constant affects heating and ageing. That is, the smaller the time constants, the faster the heating and the higher hottest-spot temperature. This, in turn, results in a higher transformer ageing rate. Fig. 17 shows the influence on ageing for 120% loading case.

The same pattern can be observed in Fig. 17. Interestingly, it can be observed that the rate-of-change of thermal constants with respect to ageing is greater than in the 90% loading case. For example, the pair $\tau_o = 90$ min. and $\tau_w = 4$ min., (*i.e.* oil constant is decreased 50% from the initial point) for the 90% loading case results in an increase of 26.3% on the ageing effect (62.3 h), whereas for the 120% loading case the increase is of 96.3% (881.5 h). This trend is increased with lower values, e.g. for the pair $\tau_o = 60$ min. and $\tau_w = 4$ min. (*i.e.* oil constant is decreased 66% from the initial point), the effect on ageing for the 90% loading case results in an increase of 53.25% (75.5 h), whereas for the 120% loading case the increase is of 229.3% (1478.8 h). This indicates a non-linear ageing impact, including a multiplicative ageing effect for the case of overload with smaller time constants.

Fig. 18 shows the HST distribution for two configurations with different time constants and different loading. The vertical line indicates the IEC hottest-spot temperature threshold value located in 98 °C.

HST values lower than the 98 °C have a mild impact on transformer ageing. However, the ageing acceleration factor impacts rapidly on the ageing after this threshold value is crossed [cf. Eq. (13)]. This can be observed in the results, namely 90% loading strategies hardly reach this threshold value and accordingly the ageing is mild. Decreasing the oil time constant leads to a more rapid heating and, therefore, higher HST. With overloading strategies, the HST is reached faster and again decreasing the oil time constant further accelerates the heating and ageing of the transformer.

4.3.3. Geographic location

For studying the effects of the geographic locations, a different site for the wind farm has been selected. The new location is at Dumat Al-Jandal in the province Al-Jouf of Saudi Arabia [48]. This location has been selected because temperatures are usually higher compared with Croatia, and this may result in higher degradation of the transformer. As for the wind resource, according to the wind roses shown in Fig. 19, it is potentially stronger in Jelinak than in Dumat Al-Jandal for the analysed period.

So as to make direct comparison between both wind farms, it has been assumed that the Jelinak wind farm was replicated in Dumat Al-Jandal. Therefore, the wind farm will have with the same characteristic power curve, but will operate in a different geographic location.

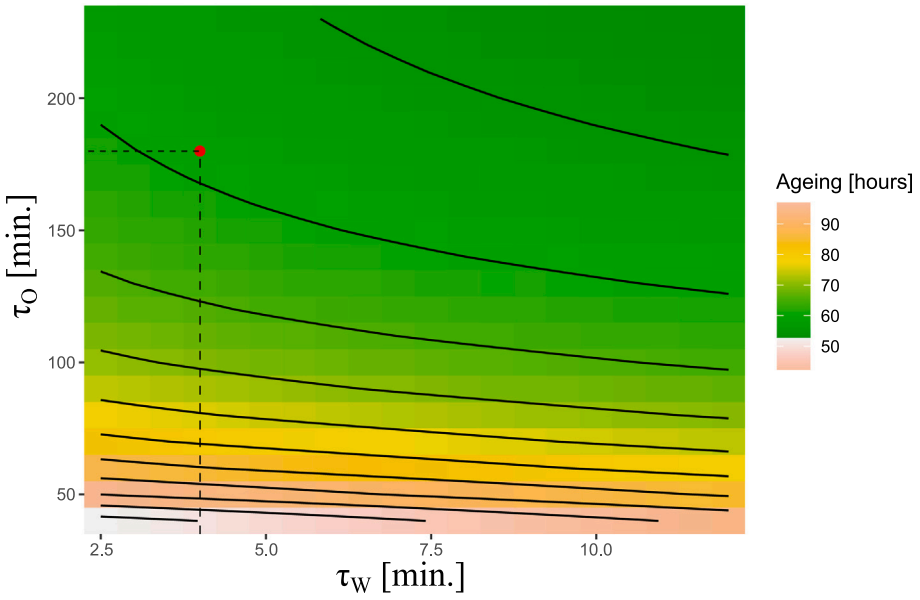

Fig. 16. Oil and winding time constants sensibility analysis — 90% loading case.

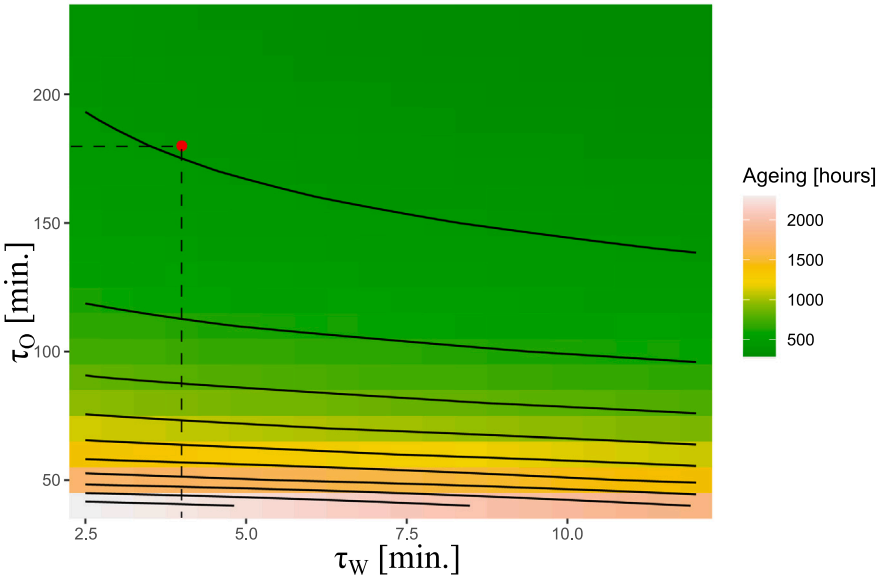

Fig. 17. Oil and winding time constants sensibility analysis — 120% loading case.

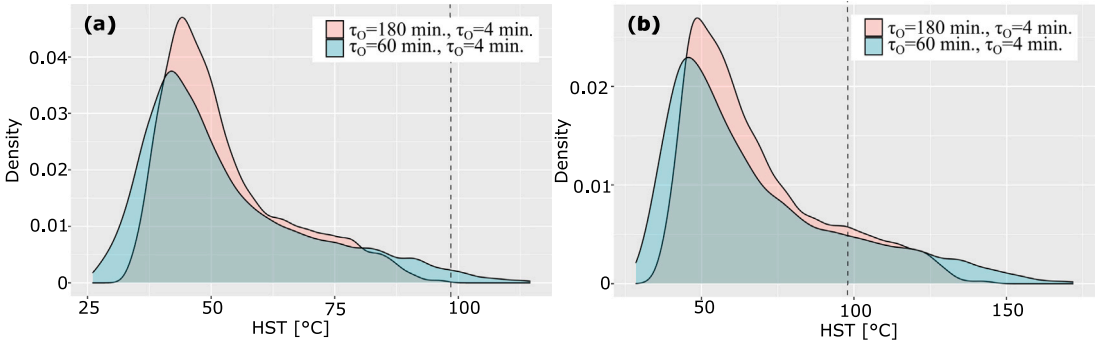

Fig. 18. HST distributions for two different thermal constants (a) 90% loading (b) 120% loading.

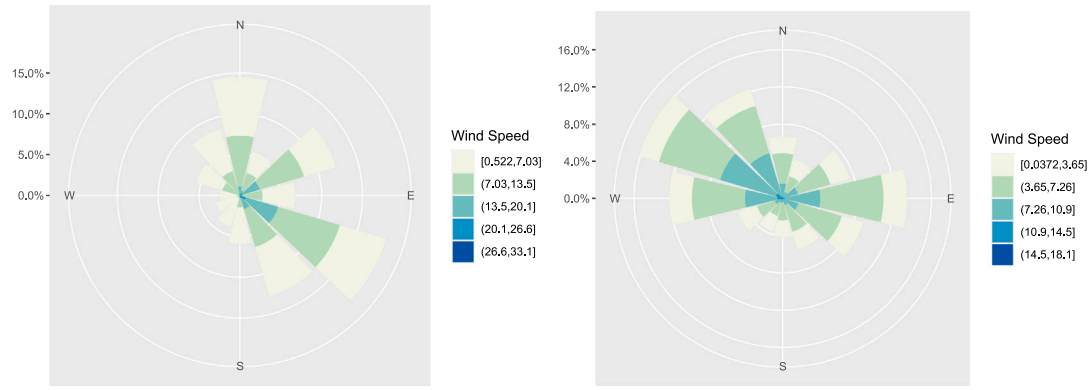

Fig. 19. Wind roses for wind farms located at Jelinak (Croatia) and al-Jandal (Saudi Arabia), period 2018–2019.

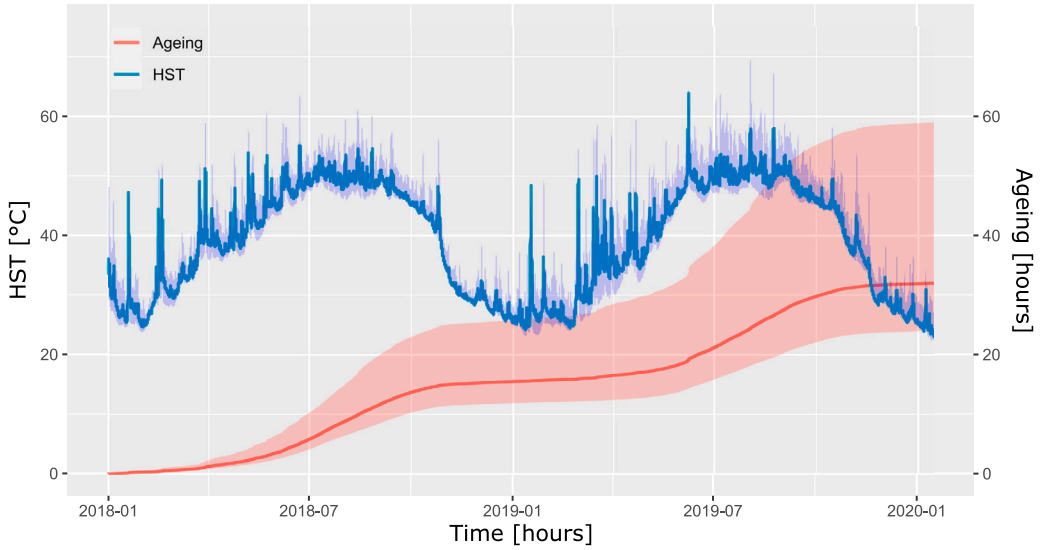

Fig. 20. Ageing of the wind farm substation transformer located at Dumat Al-Jandal for the period 2018–2019.

Meteorological data has been obtained through the ERA-5 reanalysis dataset covering the period 2018–2019 and matching Jelinak's dataset [49]. In order to obtain the wind power and transformer loading profiles, the synthetic model has been used first to create the transformer load data from the meteorological data (cf. Wind Power Modelling block in Fig. 1). Note that the domain-specific model does not need a training phase, and this is why the synthetic model has been used for this task.

The first year data has been used to design a QRF model following the same procedure for the wind farm power prediction. The following three years were used for testing and comparison. Subsequently, the ageing analysis for the available data has been performed. Fig. 20 shows the probabilistic cumulative degradation results inferred from this procedure, including the median and 95% PIs.

The median cumulative ageing and 95% PIs at the end of the testing period are of 32.1 h [23.98–59.02] h, which are greater than in the Jelinak wind farm. Despite the temperatures in Dumat Al-Jandal being higher than in Jelinak, the degradation is still small which boils down to the operation conditions (ambient temperature, wind power). Namely, Fig. 21 shows the distribution of ambient temperature, wind speed and generated power for both locations.

In Fig. 21, it can be observed that the ambient temperature distribution is wider for Dumat Al-Jandal and it is more concentrated for Jelinak and skewed to lower temperature values. As for the power, there are more no-generation instants at the Dumat Al-Jandal site than at the Jelinak site. As for the HST estimate, Dumat Al-Jandal shows a bi-modal distribution that reflects the plant operation states and Jelinak shows a centralized but stable temperature with a tendency for greater temperatures. This analysis evidences the joint impact of ambient temperature and wind power on transformer ageing. For this particular case, it happens that higher wind speed (and so higher power generation) occurs during winter when the desert temperature is very low, whereas lower wind speed occurs during summer. Thus, it can be seen that the lower power generation compensates for the higher ambient temperatures, especially during summer in Dumat Al-Jandal.

5. Discussion

A comprehensive probabilistic surrogate modelling approach has been presented in this research for transformer lifetime prediction in wind energy systems. Obtained results have shown that the proposed approach is a fast and accurate solution. The probabilistic surrogate model infers confidence bounds for transformer load, temperature and lifetime variables, which are key for transformer lifetime management.

Under the analysed design and operation conditions, the ageing of the transformer insulation is mild, which is in agreement with previous studies of transformers operated in renewable energy power plants [5]. As the prediction horizon increases, the uncertainty around the ageing prediction increases, which reflects the effect of the accumulated uncertainty over time. As for the impact of overloading strategies on ageing, a non-linear effect of the increase of loading in the transformer ageing has been observed (cf. Table 4). This is related to the hotspot

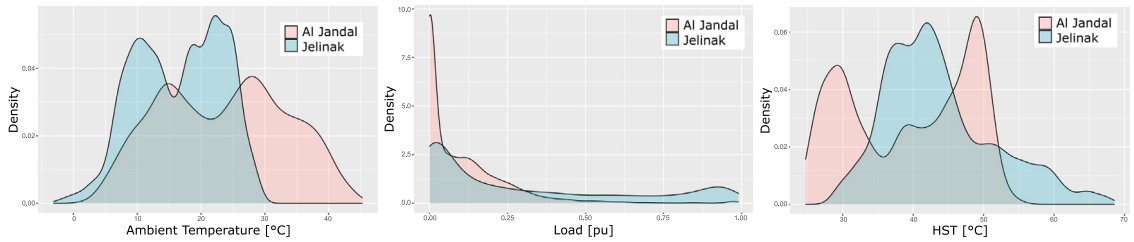

Fig. 21. Ambient temperature, power and HST distributions for Jelinak and Dumat Al-Jandal.

temperature, as after a threshold value of 98 °C defined in Eq. (13), the effect on ageing increases exponentially (cf. Fig. 18).

Transformer design parameters have been assessed though thermal constants, which are related to the transformer physical size and power rating. It can be seen that smaller transformers, as well as underrated transformers, can lead to an accelerated ageing caused by the decrease of the time constants. This evidences the importance of the thermal inertia, which is proportional to the oil mass, in preventing HST peaks that accelerate the degradation. This may establish a lower limit in volume for different power ratings instead of the core section.

The impact of the geographical location of the wind power plant has also been analysed, focusing on power plants located in Croatia and Saudi Arabia. Although intuition suggests that Saudi Arabia may have greater ageing due to the higher temperatures, it has been observed that the arid climate cools the temperature of the transformer and mitigates the insulation ageing. That is, periods of high-wind and low-temperature are interspersed with low-wind and high-temperatures. Accordingly, it can be observed that it is crucial to jointly consider transformer ageing related variables to adopt better informed decisions. This has a direct impact on dynamic transformer rating, e.g. flexibility to increase transformer loading when meteorological conditions are mild and there is a strong wind.

In order to ensure the validity of the approach for an end-to-end operation, further work is needed in testing the approach. The probabilistic surrogate model learns from observed conditions, and therefore, if the input space needs to be traversed exhaustively, different conditions need to be simulated. Accordingly, the ML model will be harder to train accurately as for longer time periods they will require more training data.

In this context, there are interesting solutions, such as generative adversarial network (GAN) based modelling techniques, which may be used to exhaustively explore and test the operation space [50,51]. In addition, the exploration of the whole input space may be prohibitive, and in this direction, it may be possible to intelligently sample to obtain fast and accurate reliability indicators [52]. Both areas are part of the future work of the authors.

6. Conclusions

Transformers are key power components for the efficient operation of power and energy systems. Their lifetime analysis is a key process for the safe, reliable and cost-efficient operation of power grids. Existing lifetime models make use of detailed and deterministic synthetic power topologies to evaluate stress and degradation, which requires high computational resources and long simulation times. The ageing trajectory of transformers operated in renewable energy applications is influenced by the stochastic behaviour of the natural resource, and accordingly, it is important to model and propagate the associated uncertainty.

In this context, this paper has presented a probabilistic machine learning aided transformer lifetime prediction framework based on probabilistic load estimation, thermal modelling and ageing analysis focused on wind energy systems. A probabilistic surrogate model has been designed for transformer load estimation, which has been connected with thermal modelling and degradation modelling stages for transformer lifetime assessment.

Namely, classical detailed transformer load estimation processes have been accelerated using an equivalent probabilistic machine learning model, which infers probabilistic load estimates with informative predictive information. Machine learning model results have been validated with real data and synthetic simulation models.

Results have shown that the performance of the machine learning models with respect to real observations are very similar, with an error margin of 0.47% for the median value and 80% prediction interval errors within 6%–7%, with a substantial reduction in the simulation time and memory requirements with respect to classical detailed simulation models.

The proposed framework was tested for a set of different load profiles, design parameters and geographic locations, resulting in consistent results that can only be interpreted by the joint-impact of the different parameters. Hence, this approach can be used for transformer health management decision-making in wind-energy systems.

Possible next steps may focus on the exhaustive and intelligent exploration of the input space for an end-to-end validation of the surrogate model.

CRediT authorship contribution statement

Jose I. Aizpurua: Conceptualization, Methodology, Sofware, Writing – original draft, Review & editing, Funding acquisition, Project administration. **Rafael Peña-Alzola:** Conceptualization, Methodology, Data curation, Writing – review & editing. **Jon Olano:** Data curation, Visualization. **Ibai Ramirez:** Data curation, Visualization. **Iker Lasa:** Resources, Writing – review & editing. **Luis del Rio:** Resources, Writing – review & editing. **Tomislav Dragicevic:** Conceptualization, Writing – review & editing.

Declaration of competing interest

The authors declare the following financial interests/personal relationships which may be considered as potential competing interests: All authors have participated in (a) conception and design, or analysis and interpretation of the data; (b) drafting the article or revising it critically for important intellectual content; and (c) approval of the final version.

This manuscript has not been submitted to, nor is under review at, another journal or other publishing venue.

The authors have no affiliation with any organization with a direct or indirect financial interest in the subject matter discussed in the manuscript

The following authors have affiliations with organizations with direct or indirect financial interest in the subject matter discussed in the manuscript:

Jose Ignacio Aizpurua, Mondragon University Ikerbasque
Rafael Peña Alzola, University of Strathclyde
Jon Olano, Mondragon University
Ibai Ramirez, Mondragon University
Iker Lasa, Ormazabal Corporate Technology
Luis del Rio, Ormazabal Corporate Technology
Tomislav Dragicevic, Technical University of Denmark

Data availability

Data will be made available on request.

Acknowledgements

This publication is part of the research projects CPP-2021-008580 funded by the Spanish Research Agency and KK-2023-00041 funded by the Basque Government, Spain. The authors from Signal Processing & Communications research group at Mondragon University are supported by the Basque Government's Research Group Program under the grant No. IT1451-22. Finally, J. I. Aizpurua is funded by Juan de la Cierva Incorporacion Fellowship, Spanish State Research Agency (grant No. IJC2019-039183-I).

References

[1] Global Wind Energy Council. Global wind report 2022. Technical report, 2022.
[2] DNV. DNV-ST-0262 — lifetime extension of wind turbines. Technical report, 2021.
[3] Veerakumar N, Ćetenović D, Kongurai K, Popov M, Jongepier A, Terzija V. PMU-based real-time distribution system state estimation considering anomaly detection, discrimination and identification. Int J Electr Power Energy Syst 2023;148:108916. http://dx.doi.org/10.1016/j.ijepes.2022.108916.
[4] Hua Y, Sun Y, Xu G, Sun S, Wang E, Pang Y. A fault diagnostic method for oil-immersed transformer based on multiple probabilistic output algorithms and improved DS evidence theory. Int J Electr Power Energy Syst 2022;137:107828. http://dx.doi.org/10.1016/j.ijepes.2021.107828.
[5] Aizpurua JI, Ramirez I, Lasa I, Rio Ld, Ortiz A, Stewart BG. Hybrid transformer prognostics framework for enhanced probabilistic predictions in renewable energy applications. IEEE Trans Power Deliv 2023;38(1):599–609. http://dx.doi.org/10.1109/TPWRD.2022.3203873.
[6] Pinciroli L, Baraldi P, Ballabio G, Compare M, Zio E. Optimization of the operation and maintenance of renewable energy systems by deep reinforcement learning. Renew Energy 2022;183:752–63. http://dx.doi.org/10.1016/j.renene.2021.11.052.
[7] Artigao E, Martín-Martínez S, Honrubia-Escribano A, Gómez-Lázaro E. Wind turbine reliability: A comprehensive review towards effective condition monitoring development. Appl Energy 2018;228:1569–83.
[8] IEC & IEEE. Power transformers - part 16: transformers for wind turbine applications. 60076-16 ed. 2.0, 2018, p. 1–26. http://dx.doi.org/10.1109/IEEESTD.2018.8476640.
[9] Heathcote MJ. J & P transformer book. 13th ed.. Newnes; 2007, http://dx.doi.org/10.1016/B978-075068164-3/50008-9.
[10] Aizpurua JI, Catterson VM, Stewart BG, McArthur SDJ, Lambert B, Cross JG. Uncertainty-aware fusion of probabilistic classifiers for improved transformer diagnostics. IEEE Trans Syst Man Cybern Syst 2021;51(1):621–33. http://dx.doi.org/10.1109/TSMC.2018.2880930.
[11] IEEE PES. IEEE guide for loading mineral-oil-immersed transformers and step-voltage regulators. IEEE std. C57.91, 2011.
[12] Suo L, Peng T, Song S, Zhang C, Wang Y, Fu Y, Nazir MS. Wind speed prediction by a swarm intelligence based deep learning model via signal decomposition and parameter optimization using improved chimp optimization algorithm. Energy 2023;276:127526. http://dx.doi.org/10.1016/j.energy.2023.127526.
[13] Wen H, Pinson P, Ma J, Gu J, Jin Z. Continuous and distribution-free probabilistic wind power forecasting: A conditional normalizing flow approach. IEEE Trans Sustain Energy 2022;13(4):2250–63. http://dx.doi.org/10.1109/TSTE.2022.3191330.
[14] Zarei T, Morozovska K, Laneryd T, Hilber P, Wihlén M, Hansson O. Reliability considerations and economic benefits of dynamic transformer rating for wind energy integration. Int J Electr Power Energy Syst 2019;106:598–606. http://dx.doi.org/10.1016/j.ijepes.2018.09.038.
[15] Daminov I, Prokhorov A, Caire R, Alvarez-Herault M-C. Assessment of dynamic transformer rating, considering current and temperature limitations. Int J Electr Power Energy Syst 2021;129:106886. http://dx.doi.org/10.1016/j.ijepes.2021.106886.
[16] Schwanka Trevisan A, Mendonça A, Gagnon R, Fecteau M, Mahseredjian J. Assessment of interactions involving wind farms in large-scale grids. Electr Power Syst Res 2021;196:107220. http://dx.doi.org/10.1016/j.epsr.2021.107220.
[17] Molina Gómez A, Morozovska K, Laneryd T, Hilber P. Optimal sizing of the wind farm and wind farm transformer using MILP and dynamic transformer rating. Int J Electr Power Energy Syst 2022;136:107645. http://dx.doi.org/10.1016/j.ijepes.2021.107645.
[18] Rosas P. Dynamic influences of wind power on the power system (Ph.D. thesis), Wind Energy Department, DTU; 2003.
[19] Slot R, Sørensen J, Sudret B, Svenningsen L, Thøgersen M. Surrogate model uncertainty in wind turbine reliability assessment. Renew Energy 2020;151:1150–62. http://dx.doi.org/10.1016/j.renene.2019.11.101.
[20] Masood Z, Khan S, Qian L. Machine learning-based surrogate model for accelerating simulation-driven optimisation of hydropower Kaplan turbine. Renew Energy 2021;173:827–48. http://dx.doi.org/10.1016/j.renene.2021.04.005.
[21] Seo J, Pokhrel J, Hu JW. Multi-hazard fragility analysis of offshore wind turbine portfolios using surrogate models. Renew Sustain Energy Rev 2022;165:112552. http://dx.doi.org/10.1016/j.rser.2022.112552.
[22] Fang J, Hu W, Liu Z, Chen W, Tan J, Jiang Z, Verma AS. Wind turbine rotor speed design optimization considering rain erosion based on deep reinforcement learning. Renew Sustain Energy Rev 2022;168:112788. http://dx.doi.org/10.1016/j.rser.2022.112788.
[23] Shadab S, Hozefa J, Sonam K, Wagh S, Singh NM. Gaussian process surrogate model for an effective life assessment of transformer considering model and measurement uncertainties. Int J Electr Power Energy Syst 2022;134:107401. http://dx.doi.org/10.1016/j.ijepes.2021.107401.
[24] Chevalier S, Schenato L, Daniel L. Accelerated probabilistic power flow in electrical distribution networks via model order reduction and Neumann series expansion. IEEE Trans Power Syst 2022;37(3):2151–63. http://dx.doi.org/10.1109/TPWRS.2021.3120911.
[25] Cremer JL, Strbac G. A machine-learning based probabilistic perspective on dynamic security assessment. Int J Electr Power Energy Syst 2021;128:106571. http://dx.doi.org/10.1016/j.ijepes.2020.106571.
[26] Duchesne L, Karangelos E, Wehenkel L. Recent developments in machine learning for energy systems reliability management. Proc IEEE 2020;108(9):1656–76. http://dx.doi.org/10.1109/JPROC.2020.2988715.
[27] Bazionis IK, Karafotis PA, Georgilakis PS. A review of short-term wind power probabilistic forecasting and a taxonomy focused on input data. IET Renew Power Gener 2022;16(1):77–91. http://dx.doi.org/10.1049/rpg2.12330.
[28] Zhang Y, Wang J, Wang X. Review on probabilistic forecasting of wind power generation. Renew Sustain Energy Rev 2014;32:255–70. http://dx.doi.org/10.1016/j.rser.2014.01.033.
[29] Abad G, Lopez J, Rodriguez M, Marroyo L, Iwanski G. Doubly fed induction machine: modeling and control for wind energy generation. IEEE press power and energy systems, Wiley; 2011.
[30] Petersson A. Analysis, modeling and control of doubly-fed induction generators for wind turbines (Ph.D. thesis), Goteborg, Sweden: Chalmers University of Technology; 2005.
[31] Aizpurua J, Stewart B, McArthur S, Penalba M, Barrenetxea M, Muxika E, Ringwood J. Probabilistic forecasting informed failure prognostics framework for improved RUL prediction under uncertainty: A transformer case study. Reliab Eng Syst Saf 2022;226:108676. http://dx.doi.org/10.1016/j.ress.2022.108676.
[32] Hu J, Heng J, Wen J, Zhao W. Deterministic and probabilistic wind speed forecasting with de-noising-reconstruction strategy and quantile regression based algorithm. Renew Energy 2020;162:1208–26. http://dx.doi.org/10.1016/j.renene.2020.08.077.
[33] Hong T, Pinson P, Fan S, Zareipour H, Troccoli A, Hyndman RJ. Probabilistic energy forecasting: Global energy forecasting competition 2014 and beyond. Int J Forecast 2016;32(3):896–913. http://dx.doi.org/10.1016/j.ijforecast.2016.02.001.
[34] Fritsch FN, Carlson RE. Monotone piecewise cubic interpolation. SIAM J Numer Anal 1980;17(2):238–46.
[35] Hersbach H. Decomposition of the continuous ranked probability score for ensemble prediction systems. Weather Forecast 2000;15(5):559–70. http://dx.doi.org/10.1175/1520-0434(2000)015<0559:DOTCRP>2.0.CO;2.
[36] IEC. Loading guide for oil-immersed power transformers. IEC 60076-7, 2018.
[37] Zou M, Holjevac N, Dakovic J, Kuzle I, Langella R, Giorgio VD, Djokic SZ. Bayesian CNN-BiLSTM and vine-GMCM based probabilistic forecasting of hour-ahead wind farm power outputs. IEEE Trans Sustain Energy 2022;13(2):1169–87. http://dx.doi.org/10.1109/TSTE.2022.3148718.
[38] Hydro-Québec. Simscape™ electrical™ reference (specialized power systems). Natick, MA: The MathWorks, Inc.; March 2022.
[39] Xu Q-S, Liang Y-Z. Monte Carlo cross validation. Chemometr Intell Lab Syst 2001;56(1):1–11.
[40] Marcot BG, Hanea AM. What is an optimal value of k in k-fold cross-validation in discrete Bayesian network analysis? Comput Statist 2021;36(3):2009–31.
[41] Penalba M, Aizpurua JI, Martinez-Perurena A, Iglesias G. A data-driven long-term metocean data forecasting approach for the design of marine renewable energy systems. Renew Sustain Energy Rev 2022;167:112751. http://dx.doi.org/10.1016/j.rser.2022.112751.
[42] Peng T, Zhang C, Zhou J, Nazir MS. An integrated framework of bi-directional long-short term memory (BiLSTM) based on sine cosine algorithm for hourly solar radiation forecasting. Energy 2021;221:119887. http://dx.doi.org/10.1016/j.energy.2021.119887.
[43] Tao Z, Zhang C, Xiong J, Hu H, Ji J, Peng T, Nazir MS. Evolutionary gate recurrent unit coupling convolutional neural network and improved manta ray foraging optimization algorithm for performance degradation prediction of PEMFC. Appl Energy 2023;336:120821. http://dx.doi.org/10.1016/j.apenergy.2023.120821.

[44] Villanueva D, Feijóo AE. Reformulation of parameters of the logistic function applied to power curves of wind turbines. Electr Power Syst Res 2016;137:51–8. http://dx.doi.org/10.1016/j.epsr.2016.03.045.

[45] Cai Y, Lim L-H. Distances between probability distributions of different dimensions. IEEE Trans Inform Theory 2022;68(6):4020–31. http://dx.doi.org/10.1109/TIT.2022.3148923.

[46] Panaretos VM, Zemel Y. Statistical aspects of Wasserstein distances. Annu Rev Stat Appl 2019;6(1):405–31. http://dx.doi.org/10.1146/annurev-statistics-030718-104938.

[47] Dai Y, Wang S, Chen X, Xu C, Guo W. Generative adversarial networks based on Wasserstein distance for knowledge graph embeddings. Knowl-Based Syst 2020;190:105165. http://dx.doi.org/10.1016/j.knosys.2019.105165.

[48] Giani P, Tagle F, Genton MG, Castruccio S, Crippa P. Closing the gap between wind energy targets and implementation for emerging countries. Appl Energy 2020;269:115085. http://dx.doi.org/10.1016/j.apenergy.2020.115085.

[49] Hersbach H, Bell B, Berrisford P, Hirahara S, Horányi A, Muñoz-Sabater J, Nicolas J, Peubey C, Radu R, Schepers D, et al. The ERA5 global reanalysis. Q J R Meteorol Soc 2020;146(730):1999–2049.

[50] Zhang J, Zhao X. Wind farm wake modeling based on deep convolutional conditional generative adversarial network. Energy 2022;238:121747. http://dx.doi.org/10.1016/j.energy.2021.121747.

[51] Xiong J, Fink O, Zhou J, Ma Y. Controlled physics-informed data generation for deep learning-based remaining useful life prediction under unseen operation conditions. Mech Syst Signal Process 2023;197:110359. http://dx.doi.org/10.1016/j.ymssp.2023.110359.

[52] Venzke A, Molzahn DK, Chatzivasileiadis S. Efficient creation of datasets for data-driven power system applications. Electr Power Syst Res 2021;190:106614. http://dx.doi.org/10.1016/j.epsr.2020.106614.